Nonstoichiometric Zinc Ferrite Nanocrystals: Syntheses and Unusual Magnetic Properties

J. F. Hochepied,[†,‡] P. Bonville,[§] and M. P. Pileni*,[†,‡]

C.E.A.-C.E. Saclay, DRECAM-S.C.M, 91191 Gif sur Yvette, Cedex, France; Laboratoire SRSI, URA CNRS 1662, Universite P et M Curie (Paris VI), BP 52, 4 Place Jussieu, 75231 Paris Cedex 05, France; and C.E.A.-C.E. Saclay, DRECAM-SPEC, 91191 Gif sur Yvette, Cedex, France

This paper demonstrates that, by using oil-in-water micelles, nonstoichiometric zinc ferrite nanoparticles are fabricated. Control in size and composition is obtained. The nanocrystals are characterized by a spinel structure with two sublattices in tetrahedral and octahedral sites. Repartition of Fe^{3+} in the two sublattices is disordered. The particles are ferrimagnetic with a noncollinear structure (the magnetic moments are not strictly parallel). This is more pronounced with the smallest particles. Zinc ferrite nanocrystals exhibit unusual magnetic properties. The anisotropy constant, K, of nanocrystals differing by their sizes is determined by Mössbauer spectroscopy and from zero field cooled (ZFC) curves. The field cooled (FC) curves show a peculiar behavior with a decrease in the magnetization at very low temperature. The ZFC curves are highly sensitive to the applied field, indicating that Langevin law cannot be applied for zinc ferrite nanocrystals. These unusual magnetic properties are attributed to the inclusion of nonmagnetic zinc ions in ferrite nanocrystals, which induces a magnetic disorder.

I. Introduction

In ferrites MFe_2O_4, the choice of M^{2+} among divalent cation (Mg^{2+}, Fe^{2+}, Co^{2+}, Ni^{2+}, Cu^{2+}, Zn^{2+}, ...) allows a relative tunability of the magnetic properties such as magnetization or anisotropy. In the spinel structure, there are twice as many octahedral (B) cationic sites as tetrahedral cationic (A) sites. If M^{2+} occupies only tetrahedral sites, the spinel is direct; if it occupies only octahedral sites, the spinel is inverse. The preferential location of M^{2+} is decisive as far as the magnetic behavior is concerned. Effectively, the exchange integrals J_{AB}, J_{BB}, and J_{AA} are generally negative and the antiferromagnetic interaction between magnetic ions in tetrahedral (A) and octahedral (B) sites is stronger than the B—B and A—A interactions.[1] The octahedral and tetrahedral sublattices are therefore antiparallel and since the number of octahedral sites is twice the number of tetrahedral sites a noncompensated magnetic moment occurs. This structure is called ferrimagnetic. If a large number of magnetic ions in tetrahedral sites are replaced by nonmagnetic ions, antiferromagnetic interactions between, on the one hand, tetrahedral and octahedral (A—B) sites and between, on the other hand, octahedral sites (B—B) leads to noncollinear structures[2–5] (the magnetic moments on B sites are not locally antiparallel to the magnetic moment in A sites). If all the tetrahedral sites are occupied by nonmagnetic ions (as Zn^{2+}), the magnetic interaction only occurs between octahedral sites. Bulk zinc ferrite was not exhaustively studied. However, Schiessl et al.[6] demonstrated that stoichiometric direct zinc ferrite presents a long-range antiferromagnetic ordering under 10 K but also a short-range ordering at higher temperatures. Similar behavior has also been observed with inclusion of nonmagnetic ions as cadmium[7] in ferrite matrix.

The size reduction of a magnetic material leads to novel properties as compared to the bulk material, due to the small volume (superparamagnetism[8]) or the high surface/volume ratio (spin canting[9,10]). A better knowledge of the behavior of magnetic particles involves basic physics (macroscopic quantum tunneling of magnetization[11]) and applied research (information storage,[12] medicine[13]).

Syntheses of ferrite nanoparticles are of great interest in the study and tailoring of specific magnetic properties. Widely used methods to fabricate nanomaterials, such as ball-milling[14,15] or coprecipitation[16–21] reaction, have been used these past two decades. More recently, new preparations have been developed as sonochemical reactions,[22] gel—sol,[23] microwave plasma,[24] and coprecipitations in reverse[25–27] and normal micelles.[28–30] This latter technique permits to fabricate nanocrystals differing by their size with no drastic change in their surface.

In ferrite nanoparticles, the magnetic ions located at the surface have fewer neighbors than in the core or in the bulk material. This disturbs the magnetic phase at the particle surface and spin-glass properties[9,10,31] are observed. The noninverted stoichiometric phase was also proven to have low ordering temperature ($T_N = 13$ K),[32] as for the bulk phase. In the past few years, several groups investigated stoichiometric zinc ferrite nanoparticles.[33–37] Changes in Fe^{3+} distribution in octahedral and tetrahedral sites induce drastic changes in the magnetic properties. Changes in the magnetization and in the ordering temperature with particle size are linked to a partial inversion of the direct spinel phase.[33]

In the past few years, a new technique to fabricate magnetic fluids made of nanocrystals has been developed in our laboratory. Functionalized oil in water (direct) micelles were used. Control in the size is obtained by a slight change in the micellar concentration. Syntheses are usually done at room temperature. Ferrites containing cobalt ions and ferrites without cobalt ions were made.[28,29,38,39] Recently it has been demonstrated for

---

* Address correspondence to this author.
† C.E.A.-C.E. Saclay, DRECAM-S.C.M.
‡ Universite P et M Curie.
§ C.E.A.-C.E. Saclay, DRECAM-SPEC.

nanoparticles having an average diameter of 3 nm, that coating with citrate does not change the magnetic properties of cobalt ferrite.[40]

In the present paper, we present for the first time fabrication of nonstoichiometric zinc ferrite nanocrystals. A solid solution of $Zn_{0.73}Fe_{2.18}\square_{0.09}O_4$ is obtained. The magnetic properties of nanocrystals differing by their sizes show unexpected behavior.

II. Experimental Section

II.1. Products. Sodium dodecyl sulfate, Na(DS), was purchased from Fluka, ferrous chloride $Fe(Cl)_2$ and cobalt acetate $Co(CH_3CO_2)_2$ were from Merck, and zinc chloride $Zn(Cl)_2$ was from Prolabo. All the compounds were stated to be 99% (minimum) pure.

II.2. Syntheses of Divalent Dodecyl Sulfate Derivatives. $Fe(DS)_2$, $Co(DS)_2$, and $Zn(DS)_2$ were prepared by stirring solutions of Na(DS) 2×10^{-2} M with a 4 times excess of ferrous chloride, cobalt acetate, and zinc chloride, respectively. By capillary ion analysis measurements it was demonstrated that these surfactants contain between 2 and 6 atom % of Na impurity. $Fe(DS)_2$, $Co(DS)_2$, and $Zn(DS)_2$ form micellar aggregates above the critical micellar concentration (cmc). For the three divalent surfactants, the cmc is nearly the same (1.4 $\times 10^{-3}$ M). The shape and the size of these aggregates were determined by small-angle X-ray scattering and by light scattering.[41] They are prolate ellipsoidal micelles with a hydrodynamic radius of 2.7 nm.

II.3. Apparatus. Transmission electron microscopy (TEM) and electron diffraction experiments were performed by using a JEOL 100CX operating at 100 kV.

Energy-dispersive spectrometry (Link AN 10 000 model) was used to analyze the samples composition.

X-ray diffraction measurements were carried out by using a Stoe Stadi P goniometer and a Siemens Kristalloflex-X-ray generator with a cobalt cathode driven by a personal computer through a Daco-PM interface.

Hysteresis loops at 3 K and zero field cooled−field cooled susceptibility measurements were performed in a commercial SQUID magnetometer.

The ^{57}Fe Mössbauer spectra were recorded using a $^{57}Co^*$: Rh γ-ray source mounted on a triangular velocity electromagnetic drive.

The particles were dispersed in PVA, with 1% mass fraction for SQUID measurements and 5% for Mössbauer measurements.

II.4. Size Determination by TEM. About 500 particles were counted to determine the size distribution. The distributions are fitted with a log-normal law[42]

$$P(D) = \frac{1}{D\sigma\sqrt{2\pi}} \exp\left(-\frac{\ln^2(D/D_0)}{2\sigma^2}\right) \qquad (1)$$

where $P(D)$ is the probability density that a particle has a diameter D, and σ and $\ln D_0$ are the standard deviation and the mean value of $\ln D$, respectively.

III. Results and Discussion

III.1. Synthesis and Characterization of Zinc Ferrite Nanoparticles with and without Cobalt Inclusions. The divalent dodecyl sulfate, $X(DS)_2$ ($X =$ Fe or Zn), is solubilized in aqueous solution (10 mL) kept at 30 °C. Methylamine is added to the mixed micellar solution which is stirred during 2 h. After centrifugation, the precipitate is washed with a solution of 50% water and 50% ethanol. After washing several times in

order to remove the surfactant, the nanoparticles are dispersed into an aqueous solution.

The iron relative percentage is kept at 75% and calculated as $[Fe(DS)_2]/\sum([X(DS)_2] = 0.75$. The methylamine concentration, $[CH_3NH_2]$, was about 1 M.

Syntheses are performed at various concentrations of ferrous dodecyl sulfate. At $[Fe(DS)_2] = 1.68 \times 10^{-2}$ M, the average particle diameter is 3.7 nm whereas at $[Fe(DS)_2] = 0.84 \times 10^{-2}$ M it is 2.8 nm.

The size distribution follows a log-normal law. The nanocrystals having the larger average diameter ($D = 3.7$ nm) are characterized by the wider size distribution ($\sigma = 0.26$) compared to the smaller ones with $D = 2.8$ nm and $\sigma = 0.22$. Hence the samples characterized by an average diameter of 3.7 nm contain a relatively large amount of nanocrystals with a rather large size (around 5 nm). This is not the case for the sample having smaller size ($D = 2.8$ nm) and narrower size distribution ($\sigma = 0.22$). We know from other studies that the magnetic properties drastically change with the particle size. The influence of the large particles is expected to have a major effect on the magnetization properties. With particles having 2.8 nm as average diameter, the contribution of large particles (5 nm diameter and more) is negligible. From this, a rather large variation in the magnetization properties is expected. This is the case even with a relatively small change in the average particle size (2.8 and 3.7 nm).

Inclusion of cobalt ions in zinc ferrite matrix is obtained by using the same experimental procedure with cobalt dodecyl sulfate as an additional parameter. The composition of cobalt dodecyl sulfate compared to zinc dodecyl sulfate, $y_s = [Co(DS)_2]/([Co(DS)_2] + [Zn(DS)_2])$, is fixed at 0.20 and 0.40. The average size of nanocrystals is 3.7 nm. The spinel structure is observed by electron and X-ray diffraction. Sample composition is determined by EDS and found equal to the relative compositions used for syntheses.

The X-ray diffraction pattern shows a spinel structure with a lattice parameter similar to the bulk phase. Therefore, the density of the material in the following studies will be taken as 5.3 g/cm^3, as in the bulk.

Composition determined by EDS is compared to the relative amount of divalent ions used to make the particles. The percentage of iron is always found to be quite constant (74% < % Fe <78%). Hence, the composition of particles is similar to the composition of the mixture used for the synthesis.

Mössbauer absorption spectra are measured in zero field in the temperature range 4.2−300 K and at 4.2 K in a 7 T transverse magnetic field.

The zero-field Mössbauer spectra of 3.7 nm particles show a transition from a blocked state at low temperature (six lines magnetic hyperfine pattern) to a superparamagnetic state at high temperature (two lines quadrupolar hyperfine pattern) (Figure 2). At 4.2 K, the spectrum has relatively narrow lines. It is slightly asymmetric due to the presence of ^{57}Fe at the tetrahedral (A) and octahedral (B) sites with slightly different hyperfine parameters. The mean hyperfine field is 508 kOe. When temperature increases, one observes a broadening of the lines and a small decrease of the hyperfine field. Up to 15 K, the thermal variation of the hyperfine field is approximately linear, in agreement with Mørup's law for an assembly of particles in the "frozen" state:[43]

$$H_{hf}(T) = H_{hf}(0)(1 - k_B T/(2K\langle V\rangle))$$

where $\langle V\rangle$ and K are the mean particle volume and the anisotropy constant, respectively. Using the mean volume derived from
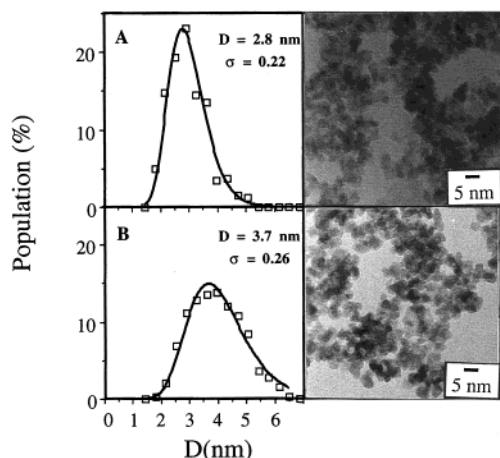
Figure 1. TEM patterns and size distributions for particles obtained in conditions $[Fe(DS)_2] = 0.84 \times 10^{-2}$ mol/L (A) and 1.68×10^{-2} mol/L (B).

Figure 3. ^{57}Fe Mössbauer absorption spectra at 4.2 K with a magnetic field applied perpendicularly to the γ-rays propagation direction in the $D = 3.7$ nm particles.
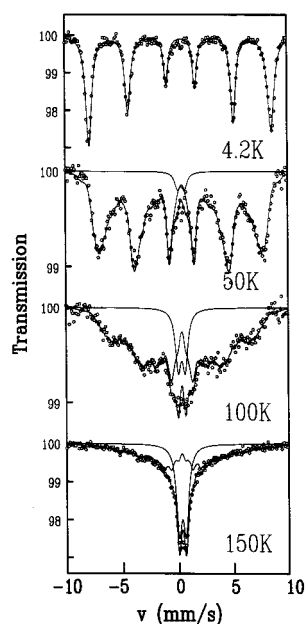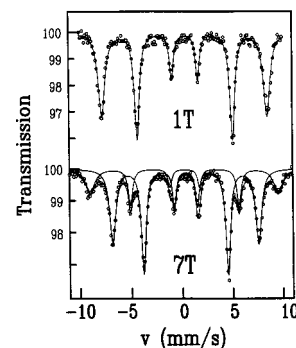

Figure 2. ^{57}Fe Mössbauer absorption spectra in zero field in the $D = 3.7$ nm particles at selected temperatures.

the TEM histograms, the anisotropy constant K, estimated from the thermal variation of the hyperfine field, is 2×10^6 erg/cm^3. The hyperfine field at 0 K, $H_{hf}(0)$, is found close to 510 kOe. Above 50 K, the magnetic hyperfine pattern is considerably broadened and the superparamagnetic doublet appears. Its relative intensity grows as temperature increases. The spectra for $T \geq 50$ K are therefore fitted to a superposition of a distribution of hyperfine fields (histogram) and of a quadrupolar doublet. The Mössbauer blocking temperature, defined as the temperature for which the magnetic sextuplet and the doublet have equal weights, is 160 K. The magnetocrystalline anisotropy constant of nonstoichiometric zinc ferrite nanocrystals is expected to be close to that of bulk γ-Fe$_2$O$_3$ ($K = +5 \times 10^4$ erg/cm^3 [44]), which is ferrimagnetic and contains only Fe^{3+} in the lattice. The anisotropy constant determined for zinc ferrite nanocrystals by Mössbauer spectroscopy is 2 orders of magnitude (2×10^6 erg/cm^3) higher than that observed for bulk γ-Fe$_2$O$_3$. This drastic enhancement is attributed to the surface anisotropy contribution for nanocrystals.[45,46] As matter of fact, it has been well described for cobalt ferrite[38,39] and γ-Fe$_2$O$_3$[47]

nanocrystals that the effective (volumic) anisotropy constant markedly increases with decreasing particle size.

To evaluate the relative repartition of iron ions in the various sites (A and B), Mössbauer spectroscopy has to be performed under a magnetic field. The Mössbauer spectra are recorded under a magnetic field H_{ext} applied perpendicular to the propagation direction of the γ-rays (transverse geometry). On increasing the applied field to 7 T, the spectra are resolved into two subspectra (Figure 3) and each subspectrum fits with a ratio I_2/I_1 close to 4. This indicates that the particles' moments are essentially aligned along the field direction. In the ferrimagnetic structure, the magnetic field tends to align the majority Fe^{3+} sublattice along its direction, and the minority sublattice opposite to it. As the hyperfine field, H_{hf}, is directed opposite to the Fe^{3+} magnetic moment, the majority sublattice must show an effective field ($H_{eff} = H_{ext} + H_{hf}$) smaller than H_{hf}, and the minority sublattice an effective field larger than H_{hf}. This is obtained with $H_{eff} = 445$ and 575 kOe for the majority and minority subspectrum, respectively. The difference between them is 130 kOe, close to the expected value for perfect alignment ($2H_{ext} = 140$ kOe). In order to derive the relative percentage of the two subspectra more accurately, hyperfine field histograms are used to account for the observed line broadening. Relative weights are 68(5)% for the majority subspectrum and 32(5)% for the minority subspectrum. Using the mean percentage values and the molecular formula Zn$_{0.73}$Fe$_{2.18}$□$_{0.09}$O$_4$ deduced from EDS, we obtain a magnetization value $M_s = 95$ emu/g if we suppose a perfect collinearity.

In conclusion, results of Mössbauer spectroscopy under field suggest a random repartition of Fe^{3+} in the two sites.

The Mössbauer spectra recorded for 2.8 nm nanosized particles are similar to those described above for 3.7 nm ones. The mean hyperfine field at 4.2 K, anisotropy constant, and blocking temperature are 504 kOe, 2.6×10^6 erg/cm^3, and 100 K, respectively.

Under the applied field the Mössbauer spectra are not as well resolved. Under an applied field of 7 T, the intensity ratio I_2/I_1 is close to 3 for both subspectra, and the relative percentages are 67(5)% for the majority subspectrum and 33(5)% for the minority subspectrum; i.e., they are the same as in the $D = 3.7$ nm particles. The broader lines and the sizable deviation from the value $I_2/I_1 = 4$ point to a rather strong angular distribution of the hyperfine fields (and hence of the Fe^{3+} moments) around the applied field. Therefore, the parallelism between the moments in the same sublattice is not verified for this sample.

III.2. Magnetic Properties. The magnetization curves, for 3.7 nm particles, measured at 3 K shows a saturation magnetization of 70 emu/g and a coercive field of 310 Oe (Figure 4). The measured saturation is lower than the calculated one from
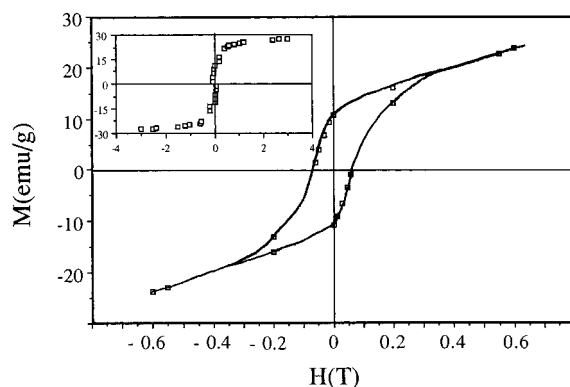
Figure 4. Hysteresis loops obtained at 3 K for nanocrystals having 3.7 nm as average size.
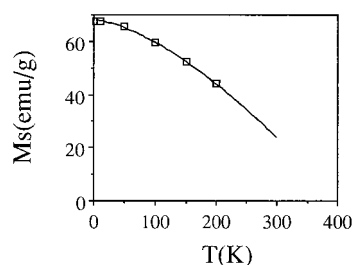

Figure 5. Thermal variation of saturation magnetization for 3.7 nm particles.

the site repartition obtained by Mössbauer spectroscopy (70 vs 95 emu/g). Such behavior has already been observed with a large number of ferrite nanoparticles and is attributed to surface spin-canting.[48] On decreasing the particle size to 2.8 nm, the saturation magnetization markedly decreases (30 emu/g). This has been already observed with other ferrite nanoparticles[49−52] and is due to an increase in the disorder of the magnetic moments orientation in the various sites when the ratio surface/volume increases.[10,48] This confirms the Mössbauer data presented above. The increase in the coercivity with decreasing the particle size (it is 650 Oe for 2.8 nm particles and 310 Oe for 3.7 nm particles) is due to the increase in the anisotropy constant with decreasing particle size. These data are in good agreement to those obtained by Mössbauer spectroscopy and observed with other nanocrystals.[38,39,47]

The thermal variation of magnetization at 5 T follows a magnon-type Bloch law for ferro- or ferrimagnets[53] (Figure 5)

$$M_s(T) = M_s(0)[1 - (T/T_0)^\alpha] \qquad (2)$$

with a T_0 value of about 400 K for 3.7 nm particles. The Bloch exponent is similar to that of the bulk phase: $\alpha = 1.5$.

In some cases with nanocrystals, the α values differ from 1.5. This was attributed to the nature of the materials, the size, and surface treatment.[54] The similarity in the Bloch exponent obtained with nanocrystals and bulk phase suggests that the surface and core of the particles are chemically and structurally identical. This is not the case when nanoparticles are fabricated by using other techniques as ball-milling.[10]

The low T_0 value indicates a decrease in Curie temperature when zinc ions are included in ferrite matrix. The magnetic interactions between the sublattices decrease and the disorder increases. Similar behavior is observed for 2.8 nm particles, with $\alpha = 1.5$ and $T_0 = 370$ K.

The ZFC−FC curves are recorded, under 10 G applied field, for particles having 3.7 nm (Figure 6A) and 2.8 nm (Figure 6B) as average diameter.
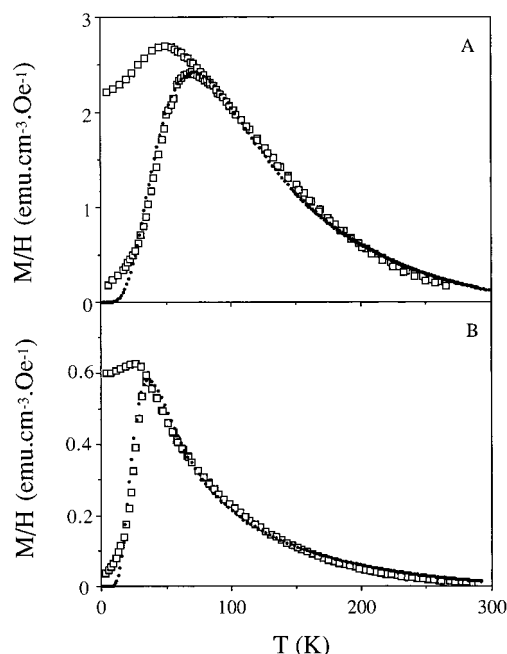

Figure 6. ZFC−FC curves for 3.7 nm (A) and 2.8 nm (B) diameter particles: (□) experimental points, (■) fit of the ZFC curve.

As expected, the ZFC magnetization increases with increasing temperature to reach a maximum and then decreases. By assuming monodisperse particles, the anisotropy constant is deduced from the maximum of the ZFC curve with the following the relationship

$$KV = kT_B \ln(\tau_m/\tau_0) \qquad (3)$$

with the measuring time $\tau_m = 100$ s and $\tau_0 = 10^{-10}$ s.

With 3.7 nm nanocrystals, the maximum of the ZFC curve is obtained at $T = 70$ K (Figure 6A). This corresponds to an anisotropy constant of 10^7 erg/cm^3. This value is very large compared to that observed by Mössbauer spectroscopy (2×10^6 erg/cm^3). This is due to the fact the volume in eq 3 is an average value deduced from the fit of the distribution with a log-normal law. In fact, larger particles have higher blocking temperatures than the smallest ones. To take into account the size distribution in the determination of the anisotropy constant, a simple model[55] is used. The ZFC curve is fitted from

$$\frac{M_{ZFC}(T)}{H} = \frac{M_s^2(T)}{k_B T} \int_0^{V_B} f(V)V^2 \, dV \qquad (4)$$

where M_{ZFC}, $M_s(T)$, V, $f(V)$, and V_B are the magnetization in the ZFC process, the saturation magnetization at temperature T, the particle volume, the particle volume distribution, and the blocking volume, respectively. The thermal variation of saturation magnetization, $M_s(T)$, is given by the Bloch law described above with $T_0 = 400$ K. The value of the particle volume distribution, $f(V)$, is chosen as close as possible as that determined by TEM. The blocking volume at temperature T is given by

$$V_B = k_B T \ln(\tau_m/\tau_0)/K$$

Equation 4 is given for particles having the easy axis in the same direction as the field. Taking into account a random distribution of the easy axis, eq 4 has to be multiplied by $\langle \cos^2 \theta \rangle = 1/3$.

Nonstoichiometric Zinc Ferrite Nanocrystals

J. Phys. Chem. B, Vol. 104, No. 5, 2000 **909**

TABLE 1: Anisotropy Constants (in 10^6 erg/cm³) Determined by ZFC Magnetization and Thermal Variation of Hyperfine Field, for Two Sizes (3.7 and 2.8 nm)

	3.7 nm	2.8 nm
ZFC	3.5	4.5
Mössbauer	2.0	2.6

It is important to note that eq 4 comes from the linearization of

$$M_{ZFC} = \int_0^{V_B} M_s V L \left(\frac{M_s V H}{k_B T} \right) f(V)\, dV \qquad (4')$$

$L(x)$ is the Langevin function $L(x) = \coth(x) - 1/x$ with $x = M_s V H / k_B T$.

The model assumes that saturation magnetization is volume independent. This is a rough approximation. As shown above and well demonstrated by other groups,[49-52] the saturation magnetization markedly changes with the particle size.

The best fit between the model and the experimental data is obtained for an anisotropy constant of 3.5×10^6 erg/cm³ (Table 1). This is in good agreement to that determined by Mössbauer spectroscopy. However, the parameters determined from the fits are far away from the experimental data. These discrepancies are as follows:

(i) The simulated diameter and standard deviation are $D = 4.4$ nm and $\sigma = 0.18$ whereas the experimental values are $D = 3.7$ nm and $\sigma = 0.26$. These discrepancies are explained by the fact that the model assumed the same saturation magnetization for various particle sizes. We know that the saturation magnetization markedly decreases with decreasing particle size. Therefore, on introducing the same saturation magnetization, the magnetic response of the small particles is overestimated and to compensate this effect the simulated size distribution contains fewer small particles. Similar behavior is observed for 2.8 nm nanoparticles with $\sigma = 0.12$ instead of 0.22 and a simulated average diameter of 3.2 nm instead of 2.8 nm.

(ii) The saturation magnetization determined from simulation is far away from that determined by high-field magnetization. Simulated values are 250 emu/g for 3.7 nm particles and 130 emu/g for 2.8 nm particles, whereas the experimental ones are 70 and 30 emu/g, respectively. No obvious explanations can be given. The ZFC magnetization curves (expressed in eq 4′) depends on the Langevin function, which is assumed to vary linearly with the low applied field. This implies no change in the ZFC curve when the applied field is low. Figure 7A shows the ZFC curves recorded at various applied fields (1–50 Oe). A perfect superposition of the M/H curves is observed both at high temperature (in the superparamagnetic regime) and at very low temperature (in the blocked state). However, the ZFC peak is more and more truncated as the field increases to reach nearly a plateau for a 50 Oe applied field (Figure 7A). This nonlinear behavior suggests the magnetization does not follow a Langevin function under low fields.

To support this conclusion, the variation of simulated reduced magnetization (M/H) with temperature is studied at various applied fields. By assuming a Langevin behavior

$$\frac{M}{H} = \frac{M_s}{H} L \left(\frac{M_s V H}{k_B T} \right) \qquad (5)$$

The simulation is done for 4 nm diameter particles having 70 emu/g as saturation magnetization.

Figure 8 clearly shows that when the particles are subjected to an applied field less than 100 Oe, the reduced magnetization
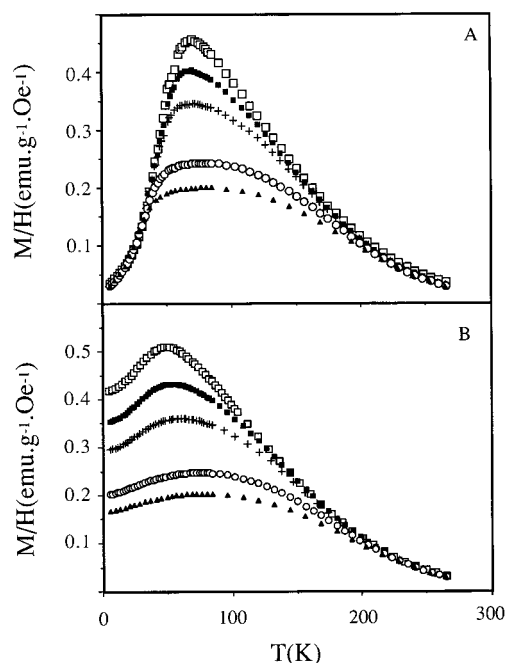

Figure 7. ZFC (A) and FC (B) curves for 3.7 nm particles in PVA 1% in mass: (□) $H = 1$ Oe, (■) $H = 5$ Oe, (+) $H = 10$ Oe, (○) $H = 30$ Oe, (▲) $H = 50$ Oe.
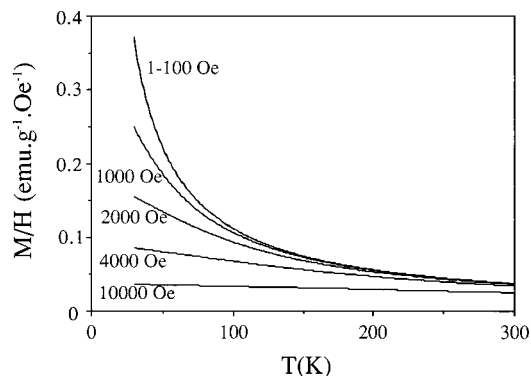

Figure 8. Langevin function versus temperature for $M_s = 70$ emu/g, $D = 4$ nm, under various fields ranging from 1 to 10000 Oe.

does not markedly change. To observe a change the applied field has to reach about 1000 Oe. This means that if magnetization follows the Langevin function, the experimental ZFC–FC curves are not expected to change when the applied field is from 1 to 100 Oe. From these data it is concluded that the Langevin law cannot be applied as usual. This behavior is rather surprising and, to our knowledge, it has never been observed before at low fields. This effect is consistent with the high simulated saturation magnetization values. The system behaves as if the magnetic energy term, $M_s V H$, in the Langevin function was considerably enhanced. This cannot be attributed to experimental errors for the following reasons:

(a) To reach such high susceptibilities, bigger volumes have to be taken into account. This has never been observed neither by TEM nor by X-ray diffraction measurements.

(b) The ratio of the saturation magnetization obtained for particles having 3.7 and 2.8 nm as diameters is very similar for simulated and experimental data.

(c) The reduced magnetizations observed in the superparamagnetic and in the frozen regions perfectly agree for various applied fields.

The applied field changes the energy required to reverse the moment along the easy axis. This could explain the fact that

the effect of the applied field is sensitive in the intermediate region between blocked and superparamagnetic regimes. Nevertheless, at the blocking temperature the anisotropy energy is still drastically higher than the thermal one. Hence this effect is expected to be insignificant as compared to the nonlinear behavior of the Langevin function.

The FC curve is recorded at various applied fields from 1 to 50 Oe. From Figure 7B, two processes are observed:

(i) A drastic drop in the magnetization with increasing the applied field. This behavior is similar to that observed with the ZFC curve. Both FC and ZFC curves follow the same evolution. As mentioned above, it can be attributed to the fact that the Langevin law cannot be applied contrary to most ferri- or ferromagnetic nanoparticles.

(ii) Whatever the applied field, Figure 7B shows an increase followed by a decrease in the magnetization with decreasing temperature. This behavior is also observed for smaller particles (2.8 nm) as shown in Figure 6B. This FC curve peak is shifted toward high temperatures when the applied field increases. The peak is observed whatever the applied field is. This demagnetization process observed by decreasing temperature remains close to 20% whatever the applied field. The presence of a peak in the FC curve at low temperature is rather surprising. As matter of fact, most of the data described in the literature[56] shows either an increase or a plateau in the magnetization with decreasing temperature. However, a peak was observed at low temperature for hematite[57] and maghemite[25] nanocrystals. In the case of hematite,[57] the authors attributed this peak to the influence of the cooling rate on the magnetic relaxation of the particles. This can be excluded in our procedure. As matter of fact, the same FC curve is recorded during warming and cooling. This shows that the phenomenon is reversible. The FC curve shape does not depend on the sample orientation. This permits to exclude any experimental errors to explain the presence of a peak in the FC curve. Another process which could explain such change in the FC curve shape could be interactions between particles. Usually, large interactions induce a plateau not far below the separation between the FC and ZFC curves without any peak. In the present experiments, the origin of the FC peak in particle–particle interactions is excluded because the same behavior is observed when particles are in powder form or when 1% in mass is dispersed in PVA. All these exclusions tend to result in another explanation which would be related to the material itself. To demonstrate this, zinc ions are replaced by cobalt.

A new parameter is defined as $y = \%\ \mathrm{Co}/(\%\ \mathrm{Co} + \%\ \mathrm{Zn})$. Nanocrystals having composition $y \leq 0.4$ are characterized by an average diameter of 3.7 nm. For $y \geq 0.6$ the size slightly decreases to 3.2 nm.

Figure 9 shows the ZFC–FC curves, recorded under 10 Oe applied field, for the three compositions $y = 0.2$, 0.4, and 1. For $y = 0.2$, Figure 9A shows a smooth FC peak compared to the sharp one observed in Figure 7B. On increasing the composition to $y = 0.4$, a slight increase in the FC magnetization on decreasing temperature (Figure 9B) is observed. In the absence of zinc ions in ferrite matrix ($y = 1$), Figure 9C shows a similar behavior as usually observed with most of magnetic nanoparticles. Hence, by a progressive replacement of zinc by cobalt ions, the FC curve tends to behave as already observed for most of the magnetic nanoparticles. It can be noted that ferrite nanoparticles containing a rather large amount of cobalt ions ($y \geq 0.6$) are characterized by a smaller size (3.2 nm) compared to that obtained at low composition (3.7 nm). This difference cannot explain the change in the FC behavior. As matter of fact, the FC curve for 2.8 nm diameter zinc ferrite
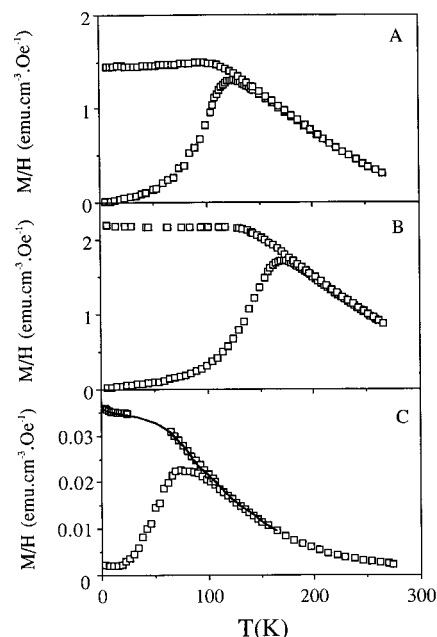

Figure 9. ZFC–FC curves for Co^{2+} substituted zinc ferrite ($D = 3.7$ nm): (A) 20% substitution; (B) 40% substitution; and (C) cobalt ferrite ($D = 3.2$ nm).

TABLE 2: Saturation Magnetization (emu/g) and Size Distribution Parameters Introduced in ZFC Fits (sim) and Obtained from Experimental Results (exp)[a]

y	0	0.20	0.40	0.60	0.75	1
M_s(exp)	68.8	74.6	62.7	30−35	30−35	30.0
M_s(sim)	250	340	415	91	50	37
D(exp)	3.7	3.8	3.8	3.3	3.0	3.2
D(sim)	4.4	3.7	4.0	3.5	3.2	3.45
σ(exp)	0.26	0.20	0.23	0.22	0.23	0.23
σ(sim)	0.18	0.15	0.12	0.18	0.22	0.18
K	3.5	17	25	11	11	8.5

[a] Deduced K values are given in 10^6 erg/cm^3.

nanocrystals shows a peak at low temperature (Figure 6B). These data tend to indicate that the maximum in the FC curve is due to inclusion of zinc ions in ferrite matrix. This could be attributed to the fact that inclusion of zinc ions induces a decrease in the magnetic interactions between the sublattices and introduces a magnetic disorder in the material.

Figure 9 shows the ZFC curve at various compositions. It is observed, for the same particle size ($y \leq 0.4$), a shift toward high temperature with increasing cobalt composition. This is due to the increase in the anisotropy constant of the material containing cobalt ions. The same model as described above (eq 4) is used to fit the ZFC curves to deduce the anisotropy constant. Table 2 shows, as expected, an increase in the anisotropy constant deduced from the fit, with increasing cobalt content at constant particle size ($y \leq 0.4$). The discrepancies between the parameters deduced from simulation and measurements vary with cobalt composition:

(i) Concerning the discrepancy in the diameter and size distribution, this was explained above by the fact the model does not take into account the change in the saturation magnetization with particle size. This is still valid at low y value where the contribution of large particles with high magnetization is rather important. At high y composition, saturation magnetization is rather low, and the average size and the percentage of large particles (around 5 nm) decrease. This permits to assume no drastic change in the saturation magnetization with particle size for samples having composition of $y \geq 0.60$. Table 2 shows

Nonstoichiometric Zinc Ferrite Nanocrystals

J. Phys. Chem. B, Vol. 104, No. 5, 2000 **911**

a rather good agreement between the experimental and simulated data at $y \geq 0.60$. This confirms the validity of the model used to determine the anisotropy constant from the ZFC curve.

(ii) Concerning the high value of the simulated compared to experimental saturation magnetization, for $y \leq 0.60$ the discrepancy remains very pronounced; for $y \geq 0.60$ the simulated magnetization is still higher than the experimental one but the discrepancy decreases progressively to become insignificant at $y = 1$. Again, these data confirm the fitting procedure is correct.

From the data it can be concluded that nonstoichiometric nanocrystals possess an unusual magnetic feature compared to other ferrite nanocrystals having the same average size. This peculiar magnetic behavior is mainly observed when the nanocrystals are subjected to a low field. This is attributed to inclusions of nonmagnetic ions (as zinc) in spinel ferrite nanocrystals, which induce a decrease in the magnetic interactions between the sublattices. This favors frustrations, that is, changes in the orientation of individual magnetic moments and an increase in the magnetic disorder. This modifies the magnetic phase under the applied field. This magnetic disorder observed with nonstoichiometric zinc ferrite nanocrystals can be linked to data observed in the bulk phase. When magnetic ions are included in ferrite phase a ferrimagnetic behavior is observed. In contrast, inclusion of nonmagnetic ions (as zinc[58-60] and cadmium[61]) induces an increase in magnetic disorder and a not well-defined ferrimagnetic behavior.

IV. Conclusion

The nonstoichiometric zinc ferrite nanoparticles exhibit a drastic size effect from 2.8 to 3.7 nm in high-field measurements as far as magnetization and coercivities are concerned. The repartition of Fe^{3+} in the two sublattices is quite disordered and the particles are ferrimagnetic with a noncollinear structure more obvious for the smaller particles.

The FC curve exhibits a peak suggesting a magnetization loss in the blocked state whose origin lies in the diluted ferrimagnetic structure of the particles, rather than the effect of sample preparation or procedure. The evaluation of the saturation magnetization by low-field susceptibility gives a value 4 times higher than in high-field measurement; this discrepancy could be related to the strong field-dependent nonlinear behavior observed at low field, showing that low-field and high-field behaviors cannot be easily correlated by simple macrospin models.

Nonstoichiometric zinc ferrite nanocrystals present particular behavior compared to other ferrite nanoparticles having similar size. This is probably due to an increase in the magnetic disorder induced by a decrease in the magnetic ions interactions between the sublattices.

References and Notes

(1) Bercoff, P. G.; Bertorello, H. R. *J. Magn. Magn. Mater.* **1997**, *169*, 314−322.

(2) Bhargava, S. C. *Phys. Rev. B* **1998**, *58*, 3240−3248.

(3) Pong, W. F.; Chang, Y. K.; Su, M. H.; Tseng, P. K.; Lin, H. J.; Ho, G. H.; Tsang, K. L.; Chen, C. T. *Phys. Rev. B* **1997**, *55*, 11409−11413.

(4) Chukalkin, Y. G.; Shtirts, V. R. *Phys. Status Solidi A* **1997**, *160*, 185−193.

(5) de Bakker, M. A.; Vandenberghe, R. E.; de Grave, E. *J. Phys. IV Fr.* **1997**, *7*, C1−267.

(6) Schiessl, W.; Potzel, W.; Karzel, H.; Steiner, M.; Kalvius, G. M.; Martin, A.; Krause, M. K.; Halevy, I.; Gal, J.; Schäfer, W.; Will, G.; Hillberg, M.; Wäppling, R. *Phys. Rev. B* **1996**, *53*, 9143−9152.

(7) Oh, H. N.; Evans, B. J. *Phys. Rev. B* **1976**, *14*, 2956.

(8) Bean, C. P.; Livingston, J. D. *J. Appl. Phys.* **1959**, *30 S*, 120S−129S.

(9) Martinez, B.; Obradors, X.; Balcells, L.; Rouanet, A.; Monty, C. *Phys. Rev. Lett.* **1998**, *80*, 181−184.

(10) Kodama, R. H.; Berkowitz, A. E.; McNiff Jr, E. J.; Foner, S. *Mater. Sci. Forum* **1997**, *235−238*, 643−650.

(11) Wernsdorfer, W.; Orozco, E. B.; Hasselbach, K.; Benoit, A.; Mailly, D.; Kubo, O.; Nakano, H.; Barbara, B. *Phys. Rev. Lett.* **1997**, *79*, 4014−4017.

(12) Sun, S.; Murray, C. B. *J. Appl. Phys.* **1999**, *85*, 4325−4330.

(13) *J. Magn. Magn. Mater.* **1999**, *194*.

(14) Goya, G. F.; Rechenberg, H. R. *J. Magn. Magn. Mater.* **1999**, *196−197*, 191−192.

(15) Fatemi, D. J.; Harris, V. G.; Browning, V. M.; Kirkland, J. P. *J. Appl. Phys.* **1998**, *83*, 6867−6869.

(16) Seki, M.; Sato, T.; Usui, S. *J. Appl. Phys.* **1988**, *63*, 1424−1427.

(17) Sato, T.; Iijima, T.; Seki, M.; Inagaki, N. *J. Magn. Magn. Mater.* **1987**, *65*, 252−256.

(18) Ueda, M.; Shimada, S.; Inagaki, M. *J. Eur. Ceram. Soc.* **1996**, *16*, 685−686.

(19) Yokoyama, M.; Sato, T.; Ohta, E.; Sato, T. *J. Appl. Phys.* **1996**, *80*, 1015−1019.

(20) Chen, Q.; Zhang, Z. J. *Appl. Phys. Lett.* **1998**, *73*, 3156−3158.

(21) Vayssières, L.; Chanéac, C.; Tronc, E.; Jolivet, J.-P. *J. Colloid Interface Sci.* **1998**, *205*, 205−212.

(22) Shafi, K. V. P. M.; Koltypin, Y.; Gedanken, A.; Prozorov, R.; Balogh, J.; Lendvai, J.; Felner, I. *J. Phys. Chem. B* **1997**, *101*, 6409−6414.

(23) Sugimoto, T.; Shimotsuma, Y.; Itoh, H. *Powder Technol.* **1998**, *96*, 85−89.

(24) Vollath, D.; Szabo, D. V.; Taylor, R. D.; Willis, J. O. *J. Mater. Res.* **1997**, *12*, 2175−2182.

(25) Lopez Perez, J. A.; Lopez Quintela, M. A.; Mira, J.; Rivas, J.; Charles, S. W. *J. Phys. Chem. B* **1997**, *101*, 8045−8047.

(26) O'Connor, C. J.; Buisson, Y. S. L.; Li, S.; Banerjee, S.; Premchandran, R.; Baumgartner, T.; John, V. T.; McPherson, G. L.; Akkara, J. A.; Kaplan, D. L. *J. Appl. Phys.* **1997**, *81*, 4741−4743.

(27) Wang, J.; Chong, P. F.; Ng, S. C.; Gan, L. M. *Mater. Lett.* **1997**, *30*, 217−221.

(28) Feltin, N.; Pileni, M. P. *Langmuir* **1996**, *13*, 3927−3933.

(29) Moumen, N.; Veillet, P.; Pileni, M. P. *J. Magn. Magn. Mater.* **1995**, *149*, 67−71.

(30) Rondinone, A. J.; Samia, A. C. S.; Zhang, Z. J. *J. Phys. Chem. B* **1999**, *103*, 6876−6880.

(31) Morrish, A. H.; Haneda, K. *J. Magn. Magn. Mater.* **1983**, *35*, 105−113.

(32) Pannaparayil, T.; Komarneni, S.; Marande, R.; Zadarko, M. *J. Appl. Phys.* **1990**, *67*, 5509−5511.

(33) Yokoyama, M.; Ohta, E.; Sato, T.; Komaba, T.; Sato, T. *J. Phys. IV Fr.* **1997**, *7*, C1−521.

(34) Ho, J. C.; Hamdeh, H. H.; Chen, Y. Y.; Lin, S. H.; Yao, Y. D.; Willey, R. J.; Oliver, S. A. *Phys. Rev. B* **1995**, *52*, 10122−10126.

(35) Hamdeh, H. H.; Ho, J. C.; Oliver, S. A.; Willey, R. J.; Oliveri, G.; Busca, G. *J. Appl. Phys.* **1997**, *81*, 1851−1857.

(36) Battle, J.; Clark, T.; Evans, B. J. *J. Phys. IV Fr.* **1997**, *7*, C1−257.

(37) Anantharaman, M. R.; Jagatheesan, S.; Malini, K. A.; Sindhu, S.; Narayanasamy, A.; Chinnasamy, C. N.; Jacobs, J. P.; Reijne, S.; Seshan, K.; Smits, R. H. H.; Brongersma, H. H. *J. Magn. Magn. Mater.* **1998**, *189*, 83−88.

(38) Moumen, N.; Pileni, M. P. *J. Phys. Chem.* **1996**, *100*, 1867.

(39) Moumen, N.; Pileni, M. P. *Chem. Mater.* **1996**, *8*, 1128.

(40) Ngo, A. T.; Bonville, P.; Pileni, M.-P. *Eur. Phys. J. B* **1999**, *9*, 583−592.

(41) Petit, C.; Lixon, P.; Pileni, M. P. *J. Phys. Chem.* **1993**, *97*, 12974.

(42) Chantrell, R. W.; Popplewell, J.; Charles, S. W. *Physica* **1977**, *86−88B*, 1421.

(43) Mørup, S.; Topsøe, H. *Appl. Phys.* **1976**, *11*, 63−66.

(44) Yang, Z.; Yao, K. *J. Appl. Phys.* **1983**, *73*, 6665.

(45) Bødker, F.; Mørup, S.; Linderoth, S. *Phys. Rev. Lett* **1994**, *72*, 282.

(46) Gazeau, F.; Bacri, J. C.; Gendron, F.; Perzynski, R.; Raikher, Y. L.; Stepanov, V.; Dubois, E. *J. Magn. Magn. Mater.* **1998**, *186*, 175−187.

(47) Prené, P.; Tronc, E.; Jolivet, J.-P.; Livage, J.; Cherkaoui, R.; Noguès, M.; Dormann, J.-L. *IEEE Trans. Magn.* **1993**, *29*, 2658.

(48) Berkowitz, A. E.; Kodama, R. H.; Makhlouf, S. A.; Parker, F. T.; Spada, F. E.; McNiff Jr, E. J.; Foner, S. *J. Magn. Magn. Mater.* **1999**, *196−197*, 591−594.

(49) Coey, J. M. D. *Phys. Rev. Lett.* **1971**, *27*, 1140.

(50) Berkowitz, A. E.; Lahut, J. A.; Jacobs, I. S.; Levinson, L. M.; Forester, D. W. *Phys. Rev. Lett.* **1975**, *34*, 594.

(51) Mollard, P.; Germi, P.; Rousset, A. *Physica* **1977**, *86−88B*, 1393−1394.

(52) Morrish, A. H.; Haneda, K. *J. Appl. Phys.* **1981**, *52*, 2496.

(53) Bloch, F. *Z. Phys.* **1931**, *61*, 206.

(54) Zhang, D.; Klabunde, K. J.; Sorensen, C. M.; Hadjipanayis, G. C. *Phys. Rev. B* **1998**, *58*, 14167−14170.

(55) Sappey, R.; Vincent, E.; Hadacek, N.; Chaput, F.; Boilot, J. P.; Zins, D. *Phys. Rev. B* **1997**, *56*, 14551−14559.

(56) Dormann, J. L.; Fiorani, D.; Tronc, E. Magnetic Relaxation in Fine-Particle Systems. In *Advances in Chemical Physics*; Prigogine, I., Rice, S. A., Eds.; John Wiley & Sons: 1997; Vol. XCVIII, pp 283−494.

(57) Zysler, R.; Fiorani, D.; Dormann, J. L.; Testa, A. M. *J. Magn. Magn. Mat* **1994**, *133*, 71−73.

(58) Dormann, J. L.; Nogues, M. *J. Phys.*: *Condens. Matter* **1990**, *2*, 1223−1237.

(59) Chukalkin, Y. G.; Shtirts, V. R. *Phys. Solid State* **1996**, *389*, 727−730.

(60) Rana, M. U.; Ul-Islam, M.; Ahmad, I.; Abbas, T. *J. Magn. Magn. Mater.* **1998**, *187*, 242−246.

(61) Ghani, A. A.; Sattar, A. A.; Pierre, J. *J. Magn. Magn. Mater.* **1991**, *97*, 141−146.